Rare Metal Materials and Engineering
Volume 55, Issue 7, July 2026
Available online at www.rmme.ac.cn

Science Press

Cite this article as: Lei Qiang, An Xinglong, Liu Xianghong, et al. Formation Mechanism of Precipitation-Free Zone in TB18 Alloy Structure[J]. Rare Metal Materials and Engineering, 2026, 55(07): 1625-1631. DOI: https://doi.org/10.12442/j.issn.1002-185X.20250359.

ARTICLE

Formation Mechanism of Precipitation-Free Zone in TB18 Alloy Structure

Lei Qiang[1,2], An Xinglong[2], Liu Xianghong[3], He Longlong[2], Zhao Gen'an[2], Shang Jinjin[1,2], Qiu Fucheng[2], Wang Tao[2], Luo Wenzhong[1,2], Lin Xin[1,2]

[1] School of Materials Science and Engineering, Northwestern Polytechnical University, Xi'an 710072, China; [2] Western Superconducting Technologies Co., Ltd, Xi'an 710018, China; [3] Northwest Institute for Nonferrous Metal Research, Xi'an 710016, China

Abstract: TB18 alloy bars were used as the research object, and the formation mechanism of the precipitation-free zone (PFZ) was investigated through microstructure characterization, composition analysis, and phase structure analysis. Results show that after solution treatment of 870 °C×120 min+aging treatment of 525 °C×240 min, discontinuous white bright spot-like pure-β PFZs exist in the middle region of the cross-section of TB18 alloy bars. During the isothermal aging, the α_s phase is preferentially precipitated and grows at the β grain boundaries. With the prolongation of aging time, PFZs are decreased to a certain extent but still remain. Composition analysis reveals that in PFZs, Mo content is relatively higher, Nb content is relatively lower, and Ti-Nb clusters exist. During solution treatment, the metastable β phase decomposes into β'' phase which is rich in β-stabilizing elements and β' phase which lacks β-stabilizing elements. The β' phase can serve as a nucleation substrate for the α phase, whereas the regions rich in β-stabilizing elements and Ti-Nb clusters will inhibit the precipitation of α phase, ultimately leading to the formation of PFZs. This study provides a theoretical basis for the process optimization of TB18 alloy.

Key words: metastable β-Ti alloy; PFZ; isothermal aging; element distribution

1 Introduction

As a new type of metastable β-titanium alloy, TB18 alloy achieves a good balance between strength (1300 MPa) and fracture toughness (70 MPa·m$^{1/2}$). The properties of TB18 alloy meet the performance requirements for main load-bearing structural materials in the new-generation aerospace vehicle models, and TB18 alloy can achieve the goals of reducing structural mass and improving structural efficiency[1–3]. Although existing studies have investigated the basic properties of TB18 alloy and their relationship with the microstructure, previous research has found that the alloy has a precipitation-free zone (PFZ) after solution-aging treatment[4–7], and there is currently no consensus on the formation mechanism of this phenomenon. PFZ may lead to fluctuations in the local properties of alloys[8–9], thereby affecting their application reliability in the key fields. Therefore, the formation mechanism of PFZ needs to be addressed urgently.

In this study, TB18 alloy bars of Φ400 mm were used as the research object. Through microstructure characterization, composition analysis, and phase structure analysis, the morphology, composition characteristics, and formation mechanism of PFZ were discussed.

2 Experiment

The research was conducted on TB18 alloy bars with diameter of 400 mm (manufactured by Western Superconducting Technologies Co., Ltd). The chemical composition of TB18 alloy is listed in Table 1. The β transformation temperature of TB18 alloy is 800±5 °C[10].

Table 1 Chemical composition of TB18 titanium alloy (wt%)

Al	Mo	V	Cr	Nb
4	5	5	5	1

Received date: July 08, 2025
Foundation item: Qin Chuangyuan Cites High-Level Innovation, Entrepreneurship Talent Project (QCYRCXM-2023-003); Innovation Capability Support Program of Shaanxi (2022KJXX-84)
Corresponding author: Liu Xianghong, Ph. D., Professor, Northwest Institute for Nonferrous Metal Research, Xi'an 710016, P. R. China, E-mail: Liu-xh@c-wst.com

The TB18 alloy ingots used in the experiment were prepared by three times of vacuum arc remelting. The master alloys used in the experiment included MoVAlCr and AlNb.

Samples were cut by wire electrical discharge machining, sequentially ground with sandpaper, mechanically polished, and finally etched in a corrosive solution composed of HF, HNO_3, and H_2O with a volume ratio of 1:3:7.

Optical microscope (OM) was used to observe the low-magnification microstructure of TB18 alloy bars. Scanning electron microscope (SEM) combined with energy dispersive spectroscope (EDS) was employed to analyze the element distribution and morphological characteristics of micro-regional structures. Transmission electron microscope (TEM) was also used for composition analysis. Atom probe tomography (APT) was used to characterize the nanoscale composition distribution.

Solution treatment (870 ℃ ×120 min) followed by isothermal aging treatment (525 ℃ ×different durations) was performed to study the evolution law of precipitate phases. The cooling method was air cooling (AC) in the whole experiment. The specific isothermal aging durations are listed in Table 2.

3 Results and Discussion

3.1 Microstructural characteristics

The metallographic structures of TB18 alloy samples after solution treatment (870 ℃ ×120 min, AC) and isothermal aging treatment (525 ℃×240 min, AC) are shown in Fig.1. To be more specific, three regions of TB18 alloy were selected for analysis: edge region, middle region, and center region. The middle region is the annulus area near $R/2$ location, where R is the radius of alloy bar. In this research, the middle region is also denoted as $R/2$ region. After heat treatment, the structure of TB18 alloy consists of equiaxed β grains with clear boundaries, presenting regular geometric polygonal contours, and the grain size is 50–200 μm. A large number of lamellar and acicular α_s phases are distributed on the supersaturated β matrix with length ranging from 100 nm to 5 μm. These α_s phases are parallel to each other, or there is a certain angle between them, indicating a strong Burgers relationship with the β matrix[11].

Table 2 Isothermal aging durations of TB18 alloy (min)

Sample	Isothermal aging duration
1	0
2	5
3	10
4	30
5	60
6	120
7	180
8	240

Meanwhile, discontinuous white bright spot zones are observed in the $R/2$ region with sizes ranging from 52 μm to 78 μm. These white bright spots are small and randomly distributed. As shown in Fig.2, α phase exists in the form of a Widmanstatten structure at the grain boundaries near the white bright spots, whereas the bright spot zones appear as PFZs.

3.2 Precipitation laws of microstructure during isothermal aging

To further understand the formation process of PFZs in TB18 alloy, samples underwent heat treatment of 870 ℃×120 min/AC+525 ℃×different durations/AC. After preparation and etching, the microstructures of the heat-treated samples are shown in Fig.3. The black area in Fig.3h is PFZ.

Since the solution temperature of TB18 alloy is much higher than the β transformation temperature, when the aging duration is less than 5 min, the microstructure still shows β grains with clear grain boundary contours, and no α phase is precipitated at this time. When the aging time is prolonged to 10 min, due to the relatively high mismatch degree at the β grain boundaries which facilitates element diffusion[12], a small number of fine α_s phases are preferentially precipitated at and near the grain boundaries, which can be regarded as the early form of uniform acicular α_s phases.

With further prolongation of the aging duration, the precipitated fine α_s phases continue to grow, leading to the coarsening of grain boundaries. Meanwhile, the content of fine α_s phases in the regions near the grain boundaries further increases. When the aging duration reaches 60 min, the α_s phases are gradually transformed into fine acicular phases, and a few α_s phases are precipitated inside the grains and near some grain boundaries. With further prolongation of the aging duration, the content of fine acicular α_s phases becomes even higher, and their distribution becomes more uniform. Most

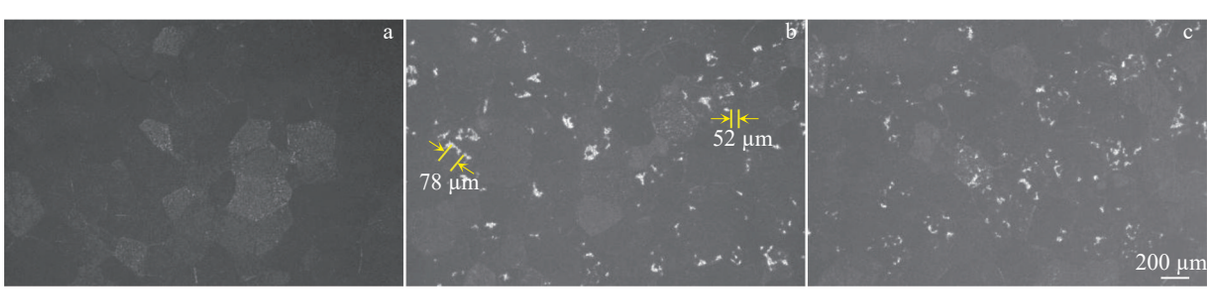

Fig.1 SEM images of TB18 alloy after heat treatment of 870 °C×120 min/AC+525 °C×240 min/AC: (a) edge region; (b) $R/2$ region; (c) center region

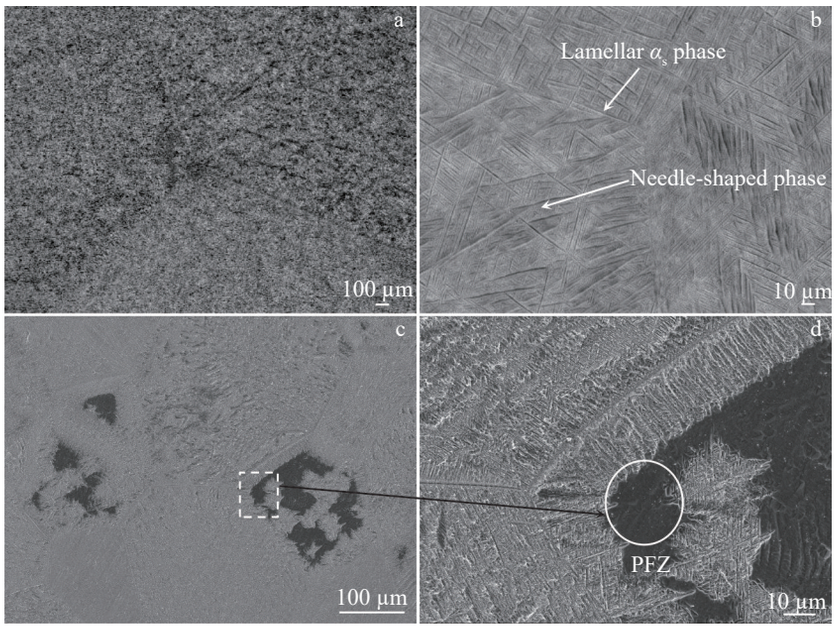

Fig.2 Microstructures of TB18 alloy after heat treatment of 870 °C×120 min/AC+525 °C×240 min/AC: (a–b) normal structures; (c–d) PFZs

intragranular PFZs are occupied by α_s phases. However, the precipitation behavior of α_s phases near certain grain boundaries is relatively weak, leading to the maintenance of a small number of PFZs.

3.3 Composition characteristics of PFZs

3.3.1 Differences in element distribution

Fig. 4 shows TEM-EDS analysis result of the composition distribution near grain boundaries in the TB18 alloy after solution treatment at 870 ℃ for 120 min followed by AC. From the edge of grain boundaries to the grain interior, the contents of elements Cr and V are basically the same with small fluctuation. At the same time, the contents of elements Mo and Nb show a little change at the grain boundaries but strong fluctuations in the grain interior.

Since both Mo and Nb are β-stabilizing elements, higher contents of Mo and Nb in the regions far from the grain boundaries are unfavorable for the precipitation of α_s phases. Due to the obvious dislocation structures at grain boundaries, dislocations can promote the precipitation of α_s phases. Therefore, α_s phases are preferentially precipitated at grain boundaries, while the fluctuations in the contents of Mo and Nb in the regions near grain boundaries affect the precipitation behavior of α_s phases.

Fig. 5 and Table 3 show APT analysis results of the composition of PFZs in TB18 alloy. It is suggested that the contents of Al, Mo, V, and Cr in PFZs differ from those in the normal regions, indicating that these elements undergo redistribution during the heat treatment process[13]. Meanwhile, the differences in the element contents, such as Al, V, and Cr, between PFZs and normal regions are relatively small (within 0.12wt%). In contrast, Mo and Nb show significant compositional differences. Particularly, Mo content in PFZs reaches 5.870wt%, which is approximately 0.660wt% higher than that in the normal regions (5.210wt%). The Nb content in PFZs is

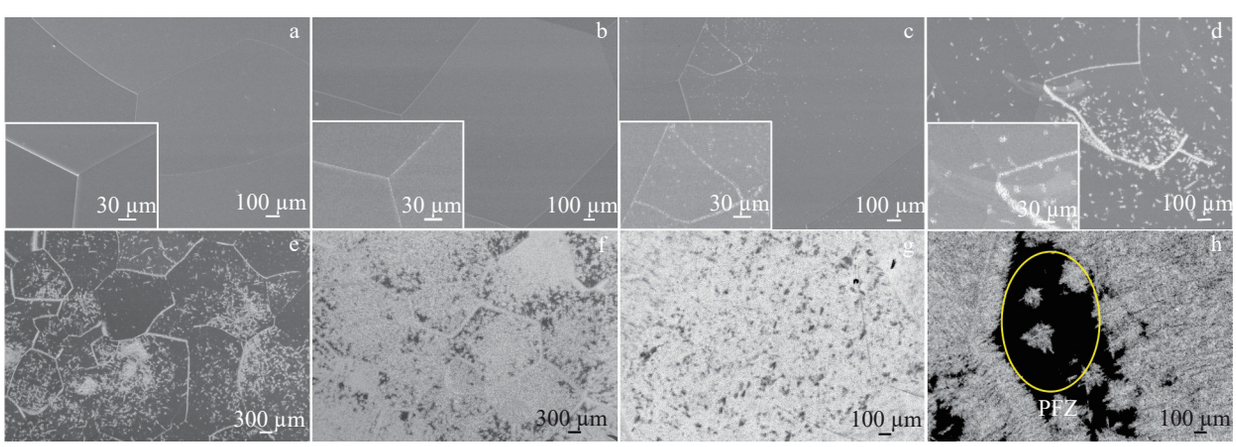

Fig.3 Precipitation evolution in TB18 alloy after heat treatment of 870 °C×120 min/AC+525 °C×different durations/AC: (a) 0 min; (b) 5 min; (c) 10 min; (d) 30 min; (e) 60 min; (f) 120 min; (g) 180 min; (h) 240 min

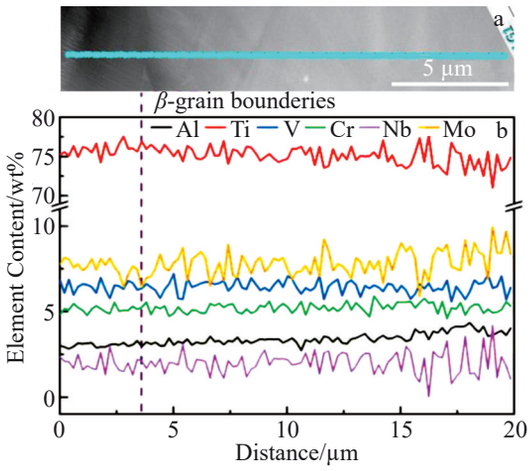

Fig.4 TEM image (a) and corresponding EDS analysis results (b) of composition near grain boundary in TB18 alloy after solution treatment at 870 °C for 120 min followed by AC

0.360wt%, which is approximately 0.640wt% lower than that in the normal regions (1.000wt%).

These results also reveal the existence of element inhomogeneity at the atomic level in TB18 alloy. The element segregation disrupts the nucleation and growth conditions of the α phase, leading to the formation of PFZs.

3.3.2 Atomic-scale segregation characteristics

The atomic densities of Mo and Nb around Ti atoms in PFZs of TB18 alloy were analyzed, and the results are shown in Fig. 6. As indicated in Fig. 6, the normalized atomic densities of Mo and Nb are both decreased with the increase in distance from Ti atoms. This phenomenon indicates that in PFZs, Mo and Nb tend to concentrate in the neighboring regions of Ti atoms, reflecting the characteristics of local segregation or short-range ordered distribution between Mo and Nb in TB18 alloy.

Around Ti atoms (distance<0.5 nm), the peak density of Nb atoms is higher (approaching 300 nm^{-3}), whereas the peak density of Mo atoms is slightly lower (approximately 250 nm^{-3}). This result shows that Nb has a more pronounced tendency for local enrichment near Ti atoms compared with Mo. This phenomenon is contrary to the overall composition of TB18 alloy, where the total content of Nb (1.000wt%) is lower than that of Mo (5.130%). This result further confirms the existence of strong Nb segregation regions adjacent to Ti atoms within PFZs.

In the medium-to-long distance range (0.5–3.0 nm) around Ti atoms, the density of Nb atoms decreases more rapidly, whereas the decrease in Mo density is relatively gradual. Beyond the distance of 1.5 nm, the overall atomic density of Mo is higher than that of Nb, which is consistent with the composition content pattern of Nb and Mo in the matrix.

Nb is strongly segregated in the regions adjacent to Ti, forming Ti-Nb clusters[14–15]. The strong Ti-Nb bonding within these clusters reduces the diffusion rate of Nb, leading to difficult concentration of elements, such as Al and O (required for α phase nucleation), at the center region. This phenomenon

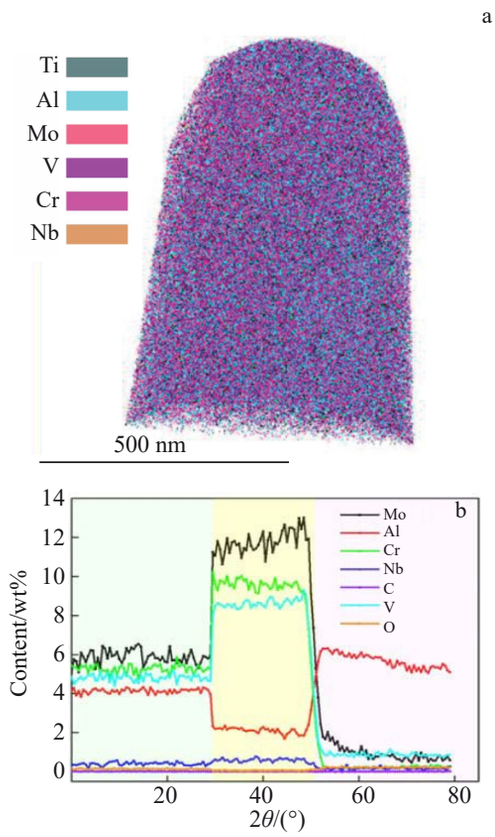

Fig.5 APT analysis results of composition of PFZ in TB18 alloy: (a) element distribution map; (b) element content

Table 3 Composition analysis results of PFZ and normal region

Element	PFZ		Normal region	
	Content/ at%	Content/ wt%	Content/ at%	Content/ wt%
Al	7.360	4.140	7.530	4.230
Mo	2.940	5.870	2.610	5.210
V	4.540	4.810	4.650	4.930
Cr	4.870	5.280	4.920	5.330
Nb	0.180	0.360	0.520	1.000
C	0.086	0.020	0.052	0.013
O	0.450	0.150	0.273	0.091
Ti	Bal.	Bal.	Bal.	Bal.

hinders the $\beta \rightarrow \alpha$ transformation, acting as a key kinetic barrier to the formation of PFZs.

3.4 Formation mechanism of PFZs

Fig. 7–Fig. 8 show TEM images and electron backscattered diffraction (EBSD) patterns of TB18 alloy after solution treatment followed by aging treatment at 525 °C for 30 and 60 min, respectively.

As shown in Fig. 7, obvious lamellar precipitate phases exist in TB18 alloy at the early stage of aging (dashed circle area in Fig. 7). According to Fig. 7b, no obvious EBSD spots of α phase can be observed, and this precipitate phase is identified as the β' phase, which has the same crystal structure as that of

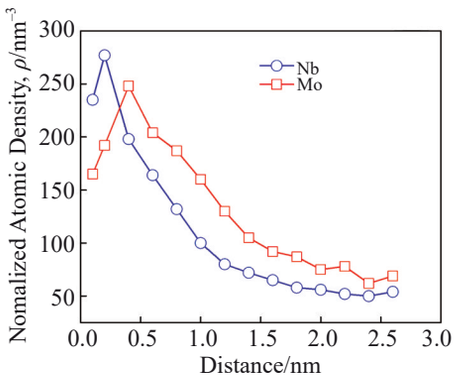

Fig.6 Normalized atomic densities of Mo and Nb around Ti atoms in PFZs of TB18 alloy

the β phase. It forms during the cooling process after high-temperature solution treatment or the early stage of aging.

The precipitation process of β' phase was analyzed with the reference to Gibbs free energy-composition curve, as shown in Fig. 9. TB18 alloy has a high content of β-stabilizing elements (approximately 16.6%, located at the right segment of the Gibbs free energy-composition curve). During solution treatment in the β phase region, alloying elements (Al, Mo, V, and Cr) fully dissolve, forming a supersaturated metastable β solid solution. In the subsequent cooling process after solution treatment, the metastable β phase decomposes into β'' phases (rich in β-stabilizing elements) and β' phases (short of β-stabilizing elements) typically through the nucleation and growth mechanism. Due to the compositional differences between the β'/β'' phases and the parent β phase, nucleation preferentially occurs at lattice defects of the parent phase (such as dislocations and grain boundaries) where energy is low and atomic diffusion is easier. For example, in the grain boundary regions with special structures which are prone to compositional fluctuations, when the distribution of β-stabilizing elements changes, the nucleation conditions for β'' phases (rich in stabilizing elements) and β' phases (short of stabilizing elements) are satisfied, leading to the formation of tiny nuclei. After nucleation, growth is achieved through atomic diffusion: β-stabilizing elements diffuse and are concentrated in the β'' phase nuclei, whereas the regions short of β-stabilizing elements develop into β' phases[16]. The transformation process can be identified as $\beta \rightarrow \beta' + \beta''$.

In TB18 alloy, if the compositional uniformity after solution treatment is inferior (or the aging conditions are suitable), pseudo-spinodal decomposition may occur[17]. In this case, the β phase decomposes spontaneously into regions rich in/short of stabilizing elements due to minor compositional fluctuations, such as local concentration differences of

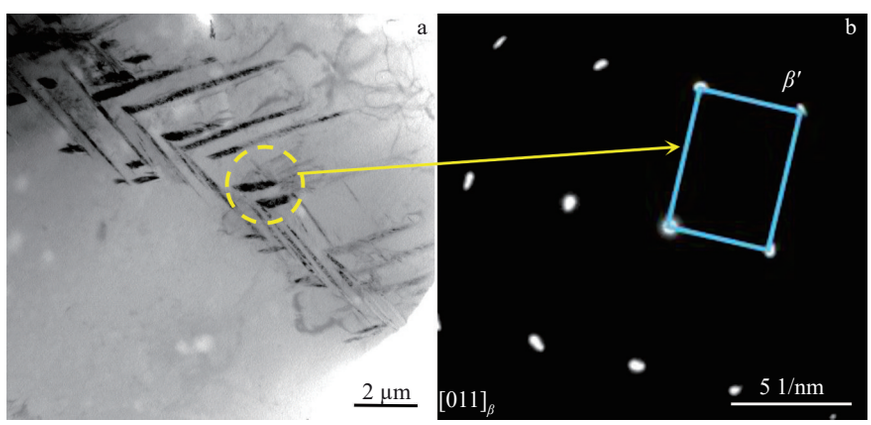

Fig.7 TEM image (a) and EBSD pattern (b) of precipitate in TB18 alloy treated by 870 °C×120 min/AC+525 °C×30 min/AC

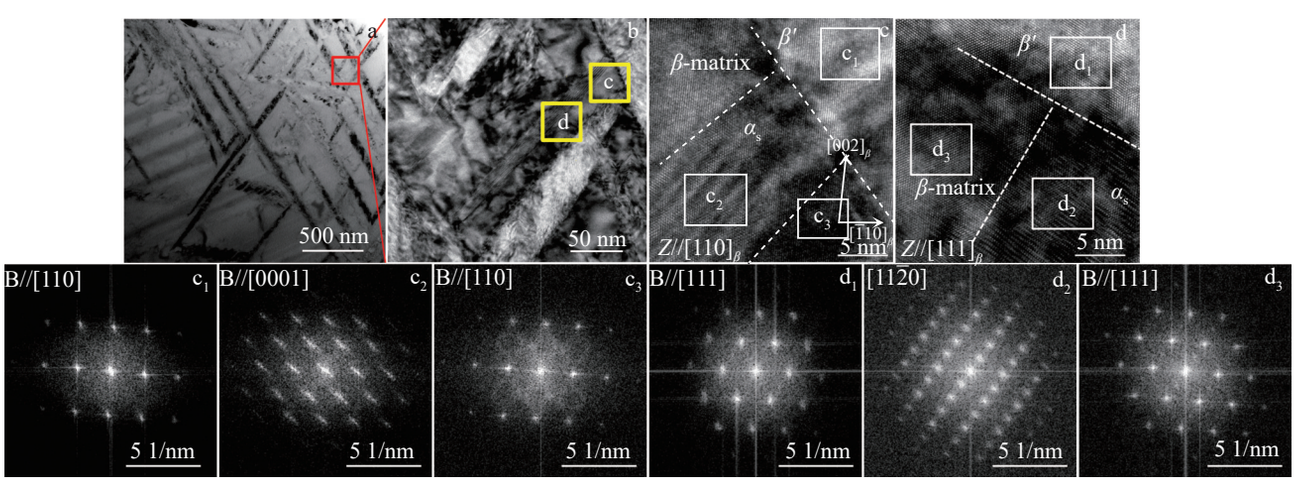

Fig.8 TEM images (a–d) and EBSD patterns (c_1–c_3, d_1–d_3) of precipitates in TB18 alloy treated by 870 °C×120 min/AC+525 °C×60 min/AC

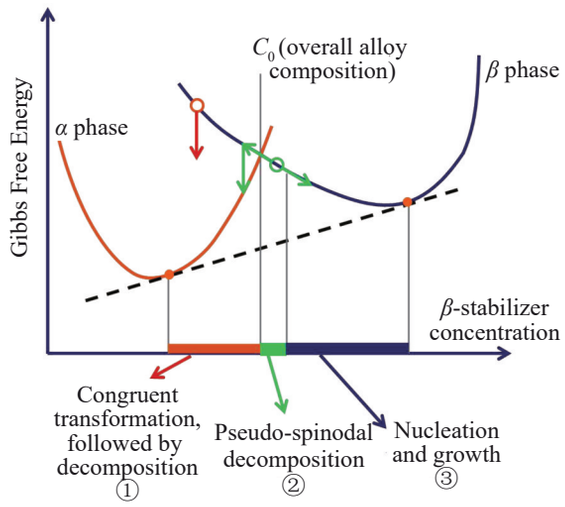

Fig.9 Gibbs free energy-composition curves

β-stabilizing elements, without obvious nucleation barriers, gradually developing into β'' and β' phases. However, compared with nucleation and growth, this decomposition is more sensitive to the initial compositional state. In TB18 alloy, it may act as an auxiliary mechanism, cooperating with nucleation and growth to accelerate phase precipitation.

The aforementioned phase segregation provides the kinetic driving force for the precipitation of the α phase during the subsequent aging process[18–19]. The β' phase, short of β-stabilizing elements, more readily meets the compositional conditions for α phase precipitation. During the subsequent aging process, secondary α lamellae are precipitated within the β' lamellae. Fig. 8 presents TEM images and EBSD patterns of TB18 alloy after solution treatment followed by aging at 525 ℃ for 60 min. As shown in Fig.8c$_2$ and 8d$_2$, the regions with B//[0001] and B//[11$\bar{2}$0] exhibit hexagonal symmetry, which is a typical characteristic of the close-packed hexagonal α phase. EBSD analysis of Fig.8 also indicates that

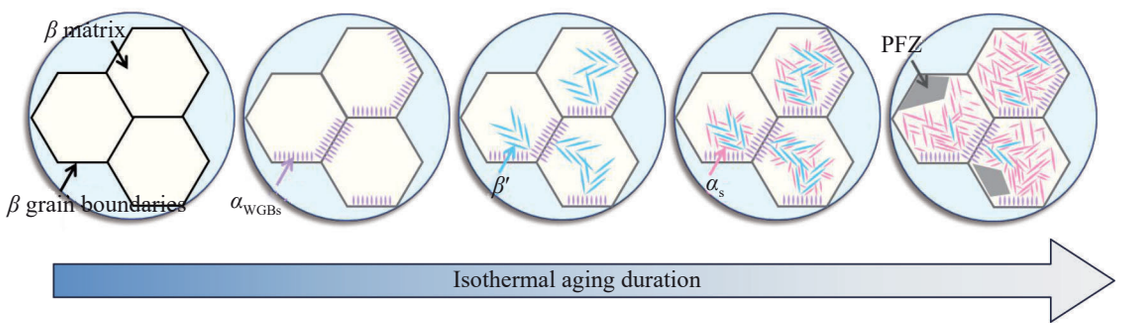

Fig.10 Schematic diagram of formation process of PFZ in TB18 alloy

β' phase, short of stabilizing elements, acts as a nucleation substrate for the α phase. With the further prolongation of aging duration, secondary α lamellae are precipitated on the broad β' phase, as shown in Fig.8c–8d.

Meanwhile, based on the analysis of the microstructure precipitation law during the isothermal aging process of the TB18 alloy (Fig. 3) and the compositional distribution characteristics of PFZs, when the secondary α phase is precipitated, the content of stabilizing elements in the β'' phase (which is rich in β-stabilizing elements) increases. Moreover, due to the compositional inhomogeneity of elements Nb and Mo, Ti-Nb clusters exist in the local regions, which further inhibit the precipitation of the secondary α phase, resulting in the formation of PFZs in local areas. Fig.10 shows the schematic diagram of the formation process of PFZ.

4 Conclusions

1) After TB18 alloy undergoes solution treatment at 870 °C for 120 min followed by isothermal aging at 525 °C for 240 min, lamellar/needle-like α_s phases are distributed in the β matrix, and a pure β-phase PFZ with width of 52–78 μm exists in the middle region of the cross-section of TB18 alloy bars.

2) During isothermal aging, the α_s phase is preferentially precipitated at β grain boundaries with high misorientation, continuously grows, and then is gradually transformed into a fine needle-like morphology. Some PFZs are retained inside partial grains or near grain boundaries; their content is decreased with the prolongation of aging duration, but PFZs still remain.

3) PFZ has a higher Mo content and a lower Nb content with the presence of Ti-Nb clusters. Element segregation disrupts the nucleation conditions of the α phase.

4) During solution treatment, the β phase decomposes into β' (short of β-stabilizing elements) and β'' (rich in β-stabilizing elements) phases. The β' phase promotes the precipitation of the α phase, whereas the β'' phase and Ti-Nb clusters inhibit α phase precipitation, ultimately leading to the formation of PFZs.

References

1 Shang Guoqiang, Zhu Zhishou, Chang Hui *et al*. *Rare Metals*[J], 2011, 35(2): 286 (in Chinese)
2 Yang Dongyu, Fu Yanyan, Hui Songxia *et al*. *Rare Metals*[J], 2011, 35(4): 575 (in Chinese)
3 Qian Jiuhong. *Rare Metals*[J], 2000, 24(3): 218 (in Chinese)
4 Li Shaoqiang, Gong Zhanpeng, Li Hui *et al*. *Rare Metal Materials and Engineering*[J], 2020, 49(9): 3045 (in Chinese)
5 Zhou W, Liu X H, Feng J *et al*. *Rare Metal Materials and Engineering*[J], 2022, 51(9): 3129

6 Hu Shengshuang, Chen Suming, Yan Jiawei *et al*. *Heat Treatment to Metals*[J], 2024, 49(2):190 (in Chinese)
7 Li Bo, Qin Fengying, Lin Yuan *et al*. *Transactions of Materials and Heat Treatment*[J], 2025, 45(2): 122 (in Chinese)
8 Li Bo, Xiang Wei, Zhang Feng *et al*. *Heat Treatment of Metals* [J], 2024, 49(5):106 (in Chinese)
9 He Yongdong, Chen Ming'an, Zhang Xinming *et al*. *Rare Metal Materials and Engineering*[J], 2009, 38(12): 2093 (in Chinese)
10 Zhou Wei, Xin Shewei, Liu Xianghong *et al*. *Titanium Industry Progress*[J], 2023, 40(5): 440 (in Chinese)
11 Zhu W G, Lei J, Tan C S *et al*. *Materials & Design*[J], 2019, 168: 107640
12 Liu Xianghong, Zhao Ning, Wang Tao *et al*. *Rare Metal Materials and Engineering*[J], 2024, 53(11): 3101
13 Ouyang Delai, Xie Youmei, Hu Shengwei *et al*. *Rare Metal Materials and Engineering*[J], 2023, 52(2): 710 (in Chinese)
14 Song Zhiru, Song Mengfan, Wang Qing *et al*. *Transactions of Materials and Heat Treatment*[J], 2025, 46(3): 84 (in Chinese)
15 Du Zhaoxin. *Study on Heat Treatment, Microalloying and High-Temperature Deformation Behavior of New High-Strength β Titanium Alloys*[D]. Harbin: Harbin Institute of Technology, 2014 (in Chinese)
16 Luo Yuanyuan. *Study on Phase Transformation During Aging Process of Ti-B19 Titanium Alloy*[D]. Xi'an: Northwestern Polytechnical University, 2006 (in Chinese)
17 Ricard A, Pietro T, Jaume C. *Nature Communications*[J], 2016, 7: 13067
18 Chang Hui. *Kinetics of Solid-State Phase Transformation and Its Microstructural Evolution Law in Ti-B19 Alloy*[D]. Xi'an: Northwestern Polytechnical University, 2006 (in Chinese)
19 Yin Y F, Zhao B, Jia W J *et al*. *Rare Metal Materials and Engineering*[J], 2019, 48(9): 3001

TB18合金组织无析出区的形成机理

雷　强[1,2]，安星龙[2]，刘向宏[3]，何龙龙[2]，赵根安[2]，尚金金[1,2]，邱富城[2]，王　涛[2]，罗文忠[1,2]，林　鑫[1,2]
(1. 西北工业大学 材料学院，陕西 西安 710072)
(2. 西部超导材料科技股份有限公司，陕西 西安 710018)
(3. 西北有色金属研究院，陕西 西安 710016)

摘　要：以TB18合金棒材为对象，通过显微组织表征、成分分析及相结构分析，探究未析出区的形成机理。结果表明：经870 ℃×120 min固溶+525 ℃×240 min时效处理后，TB18合金棒材横截面中间以内区域存在不连续白色亮斑状纯β相无析出区；在等温时效过程中，α_s相优先在β晶界析出并长大，部分无析出区随时效时间增加有所减少但仍有保留。成分分析显示，无析出区中Mo含量偏高、Nb含量偏低，且存在Ti-Nb团簇；固溶时，亚稳β相分解为富β稳定元素的β''相和贫β稳定元素的β'相，β'相可作为α相形核衬底，而富β稳定元素区域及Ti-Nb团簇会抑制α相析出，最终形成无析出区。本研究为TB18合金工艺优化提供理论依据。

关键词：亚稳态β钛合金；无析出区；等温时效；元素分布

作者简介：雷　强，男，1985年生，硕士，高级工程师，西部超导材料科技股份有限公司，陕西 西安 710018，E-mail：hutu511@c-wst.com